Applicability of active infrared thermography for screening of human breast: a numerical study

Geetika Dua
Ravibabu Mulaveesala

Applicability of active infrared thermography for screening of human breast: a numerical study

Geetika Dua and Ravibabu Mulaveesala*
Indian Institute of Technology Ropar, InfraRed Imaging Laboratory, Department of Electrical Engineering, Rupnagar, Punjab, India

Abstract. Active infrared thermography is a fast, painless, noncontact, and noninvasive imaging method, complementary to mammography, ultrasound, and magnetic resonance imaging methods for early diagnosis of breast cancer. This technique plays an important role in early detection of breast cancer to women of all ages, including pregnant or nursing women, with different sizes of breast, irrespective of either fatty or dense breast. This proposed complementary technique makes use of infrared emission emanating from the breast. Emanating radiations from the surface of the breast under test are detected with an infrared camera to map the thermal gradients over it, in order to reveal hidden tumors inside it. One of the reliable active infrared thermographic technique, linear frequency modulated thermal wave imaging is adopted to detect tumors present inside the breast. Further, phase and amplitude images are constructed using frequency and time-domain data analysis schemes. Obtained results show the potential of the proposed technique for early diagnosis of breast cancer in fatty as well as dense breasts. © *2018 Society of Photo-Optical Instrumentation Engineers (SPIE)* [DOI: 10.1117/1.JBO.23.3.037001]

1 Introduction

Infrared thermography (IRT) has proved to be an important screening tool for early diagnosis of various diseases such as diabetes, thyroid, skin cancer, breast cancer etc. Nowadays, breast cancer is one of the major disease affecting women worldwide. It is a curable disease with higher chances of survival if diagnosed in its early stages.[1–3] Among different medical imaging modalities like mammography, ultrasound, and magnetic resonance imaging, mammography is known to be a widely used method for detecting breast cancer. But this method shows its limitations in detecting tumors present in the dense breast. Dense breasts have less fat and more gland tissue in comparison to the fatty breasts, which restricts mammography to detect tumors easily. Also, mammography provides discomfort to the patient and the exposure to harmful ionizing radiation limits its applicability. So, in this respect, IRT outperforms the standard method of mammography by providing patient friendly diagnostic technique.

IRT is a non-invasive, noncontact diagnostic tool that is economic, quick, radiation free, and painless to the patient. It is rather a precise imaging method that detects the temperature variations on the surface of the human skin. The tumor cells have a higher temperature than the normal cells due to their high metabolic activity. IRT is hence well suited to detect asymmetrical temperature distributions as well as the presence of hot and cold spots, which indicates subsurface abnormalities.

The present work highlights a simulation study for the identification of tumors at an early stage in dense as well as in fatty breasts. It can be implemented in two ways: either in passive or active.[4–10] The preferred approach is passive, as it does not involve any active heating or cooling of the breast. However,

with passive approach, the obtained sensitivity is not enough unless an external energy (heating or cooling) source is utilized to create significant thermal contrast on the skin surface.[7–10] The present study is emphasized on an active thermography technique to detect tumors with significant thermal contrast over the breast. In this approach, an external thermal stimulus from the heat source is directed towards the breast to be inspected for creating temperature differences in the infrared images. The thermal stimulus can be applied either in a pulsed form (pulse and pulse-phase thermography) or in a harmonic modulated way (lock-in thermography). Pulse thermography (PT) demands a higher peak power heat source and has the additional drawback of nonuniform heating.[5] In lock-in thermography (LT), to detect the abnormalities present at different depths in the test specimen, repetition of the experiment is required, which makes it a time consuming process.[6] In pulse phase thermography (PPT), though the experimental procedure is similar to PT, the postprocessing is performed using Fourier transform resulting in both amplitude and phase of the obtained thermal response over the surface of the test specimen.[4] But still, the demand of high peak power heat sources remains.[7]

In order to overcome some of the traditional limitations with the aforementioned conventional thermographic techniques (peak power, resolution, and depth of penetration), the present work focuses on linear frequency modulated thermal wave imaging (LFMTWI).[7–10] In contrast to lock-in thermography, varying depth resolution can be achieved in frequency modulated thermal wave imaging by probing band of wavelengths. This band of wavelengths is directly decided by the modulation frequencies obtained from the heat source, leading to the detection of tumors present at different depths in the breast. Using LFMTWI technique, a frequency-modulated heat stimulus

*Address all correspondence to: Ravibabu Mulaveesala, E-mail: ravibabucareiitd@yahoo.co.in

with frequencies varying within a predefined band having equal magnitude is imposed over the breast. Thermal waves generated due to applied heat stimulus diffuse into the breast and produce a similar temporal temperature distribution on the skin surface of the breast. The presence of tumors inside the breast alters the heat flow resulting in temperature gradients over the surface. This resultant thermal response over the skin surface of the breast is recorded and further processed using Fourier transform and matched filter approach.[8–14]

2 Theory

Postprocessing approaches adopted frequency domain (magnitude and phase) and time domain (matched filter), which are described in Secs. 2.1 and 2.2.

2.1 Fourier Transform Approach

The frequency-domain analysis (mangnitude and phase information) has been carried out on the recorded thermal response over the skin surface using discrete Fourier transform (DFT). One dimensional DFT is computed for each pixel on the zero mean (mean removed) temperature distribution $[T_{\text{mean removed}}(x, y, t)]$ (where x, y are the spatial coordinates, and t is the index of image sequence) in the field of view as

$$T(x, y, k) = \sum_{n=0}^{N-1} T_{\text{mean removed}}(x, y, t) e^{-\frac{j2\pi kn}{N}}$$
$$= \text{Re}[T(x, y, k)] + j\,\text{Img}[T(x, y, k)], \quad (1)$$

where k is the bin number, N is the total number of frames, $\text{Re}[T(x, y, k)]$ and $\text{Img}[T(x, y, k)]$ are the real and imaginary parts of the $T(x, y, k)$.

The magnitude images are then reconstructed from the computed real and imaginary components as

$$|T(x, y, k)| = (\{\text{Re}[T(x, y, k)]\}^2 + \{\text{Img}[T(x, y, k)]\}^2)^{1/2}. \quad (2)$$

Further, the phase images are reconstructed using the real and imaginary components as

$$\angle T(x, y, k) = \tan^{-1}\left\{ \frac{\text{Img}[T(x, y, k)]}{\text{Re}[T(x, y, k)]} \right\}. \quad (3)$$

2.2 Matched Filter Approach

A matched filter approach is based on the assumption of complex signals. The thermal response obtained on the skin surface is a real signal. So, it is convenient to transform this real temperature signal to a complex form. This complex form can then be matched and used to compute phase and amplitude information. To achieve this, Hilbert transform is applied to create an "analytic signal." The Hilbert transform $H[T_{\text{mean removed}}(x, y, t)]$ of a mean removed thermal signal $[T_{\text{mean removed}}(x, y, t)]$ to construct the analytic signal is defined as

$$x_h(t) = H[T_{\text{mean removed}}(x, y, t)]$$
$$= \frac{1}{\pi} \int_{-\infty}^{+\infty} \frac{T_{\text{mean removed}}(x, y, \tau)}{t - \tau} d\tau, \quad (4)$$

$$= T_{\text{mean removed}}(x, y, t) * \frac{1}{\pi t}. \quad (5)$$

Thus, Hilbert transform $x_h(t)$ of $T_{\text{mean removed}}(x, y, t)$ can be described as the convolution (*) of $T_{\text{mean removed}}(x, y, t)$ with the signal $1/\pi t$. From this, the analytic signal is obtained as

$$x_a(t) = T_{\text{mean removed}}(x, y, t) + jx_h(t). \quad (6)$$

The phase information is then calculated as

$$\phi(t) = \tan^{-1} \frac{x_h(t)}{T_{\text{mean removed}}(x, y, t)}. \quad (7)$$

Further, the amplitude or correlation coefficient (CC) images are constructed using

$$\text{CC}(t) = T_{\text{mean removed}}(x, y, t) \Theta x_{\text{ref}}(x, y, t), \quad (8)$$

where $x_{\text{ref}}(x, y, t)$ is chosen reference thermal signal, and "Θ" denotes the circular convolution operator.

This approach concentrates the total applied energy into a narrow duration pulse using matched filtering and improves depth resolution.

3 Method

The proposed work deals with the numerical modeling of fatty and dense breast tissues using finite element method. Two three-dimensional (3-D) models of human breast (one showing dense breast and other being a fatty breast) are created as the semiellipsoid multilayered structures with seven tissue layers (epidermis, papillary dermis, reticular dermis, fat, gland, muscle, and chest wall) having different thermophysical properties.[15–20] Thermophysical properties of the mentioned layers are given in Table 1.[15–17] Both the models (dense and fatty) are different in terms of fat and gland layer thickness. Models are generated with a normal mesh using tetrahedral elements to illustrate quantitative thermal analysis of breast cancer.

Here, k is the thermal conductivity, ρ is the density, c is the specific heat, Q_m is the metabolic heat generation rate, and ω_b is the blood perfusion rate.

A typical schematic of the experimental setup for the proposed numerical study of active frequency modulated thermal

Table 1 Thermophysical properties of different tissue layers.[15–17]

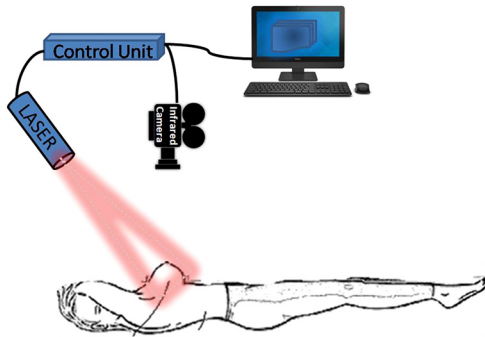| Tissue layer	k (W/m.K)	ρ (kg/m³)	c (J/kg.K)	Q_m (W/m³)	ω_b (m³/s/m³)
Epidermis	0.235	1200	3589	0	0
Papillary dermis	0.445	1200	3300	368.1	0.0002
Reticular dermis	0.445	1200	3300	368.1	0.0013
Fat	0.21	930	2770	400	0.0002
Gland	0.48	1050	3770	700	0.0006
Muscle	0.48	1100	3800	700	0.0009
Chest wall	0.48	1100	3800	700	0.0009
Tumor	0.48	1050	3852	10,000	0.012

Fig. 1 Schematic of the typical experimental arrangement for the frequency modulated thermal wave imaging for breast cancer screening.

wave imaging is as shown in Fig. 1. The source control unit controls dynamic heating and also synchronizes the camera data capturing (thermograms capture rate). To test the capability of LFMTWI approach, the 3-D finite element analysis (FEA) is performed by considering two different types of external heat fluxes, i.e., LFM (LFMTWI) and a pulse (PT) type heat fluxes. The results are computed for both the approaches (LFMTWI and PT) and further compared to prove the potential capabilities of the proposed approach.

In case of LFMTWI, the 3-D FEA is performed by imposing an LFM heat flux of 40 W/m^2 with frequency sweep of 0.002 to 0.02 Hz for duration of 500 s over the skin surface of both the modeled breast samples. The imposed LFM heat flux is as shown in Fig. 2.

In case of PT, a pulse signal of duration 300 s by keeping the average energy same as that of the LFM excitation signals imposed over the skin surface of both the modeled breast samples (dense and fatty). The schematic of the imposed pulsed heat flux is as shown in Fig. 3.

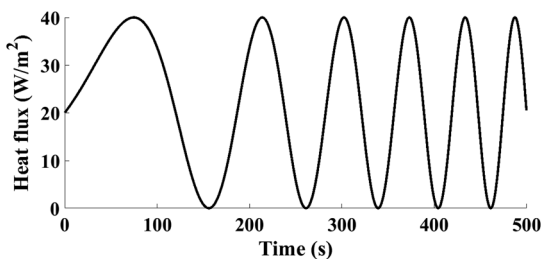The process of heat transfer in breast tissues is described using Pennes bioheat equation as[1–3]
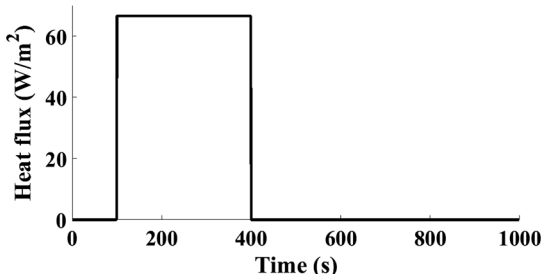

Fig. 2 The imposed LFM heat flux.

Fig. 3 The imposed pulsed heat flux.

$$\rho.c\frac{\partial T}{\partial t} = \nabla(k.\nabla t) + \omega_b.c_b.\rho_b(T_a - T) + Q_m, \qquad (9)$$

where ρ_b and c_b are density and specific heat of the blood, respectively, ω_b is the blood perfusion rate, T_a is the arterial blood temperature, T is the local temperature of the breast tissue, and Q_m is the metabolic heat generation rate. The density and the specific heat of blood are taken to be as 1055 kg/m^3 and 3660 J/kg.K, respectively. The arterial blood temperature is considered to be the core temperature of the human body, i.e., 310.15 K. The resultant thermal response over the surface of the skin is captured at a rate of 5 frames per second. Additive white Gaussian noise (AWGN) with signal to noise ratio (SNR) of 30 dB is artificially added to the captured data for testing the detection capabilities of the proposed technique in presence of noise (i.e., in real-time experiments). The constructed noisy thermal data are further processed to obtain a zero mean thermal profile by fitting the temporal temperature data with an appropriate polynomial.

4 Results and Discussions

Obtained thermal responses over the breast (both fatty and dense breasts) have been processed and analyzed using frequency-domain (Fourier transform) and the time-domain (matched filter) approaches in the following sections:

4.1 Modeling and Analysis of the Dense Breast Tissue

The schematic of the modeled dense breast is as shown in Fig. 4. Fat layer has a thickness of 2 mm and gland has thickness of 45 mm. Four tumors (denoted as a, b, c, and d in Fig. 4) each with 20 mm diameter are artificially kept at different locations inside the gland layer of the breast.[18–21] Each tumor is placed at different depths in order to test the resolution capabilities of the proposed approach.

The respective depths of tumors from the top surface are as given in Table 2.

Resultant images are constructed for both the approaches (LFMTWI and PT) and results are further compared by considering SNR as a figure of merit.

Image constructed from the fitted noisy data for dense breast is as shown in Fig. 5(a) using LFMTWI and Fig. 5(b) using PT. The obtained results for the dense breast after processing zero mean noisy thermal data are as shown in Figs. 6–9. Figures 6(a) and 6(b) represent the phase images obtained at a frequency of 0.004 Hz reconstructed by applying Fourier transform on the fitted noisy temporal temperature profiles for LFMTWI and PT, respectively.

Figure 7 shows the amplitude images obtained at a frequency of 0.004 Hz reconstructed by applying Fourier transform on the fitted noisy temporal temperature profiles for both the approaches. Figure 7(a) shows the reconstructed image using LFMTWI and Fig. 7(b) using PT.

The phase and amplitude (CC) images constructed as a result of matched filter approach are shown as Figs. 8 and 9. The phase image as shown in Fig. 8(a) is obtained at 333 s using LFMTWI, and Fig. 8(b) is obtained at 543 s using PT approach whereas the amplitude image [Fig. 9(a)] is obtained at 21 s for LFMTWI and Fig. 9(b) obtained at 822 s for PT.

Results are further compared using SNR as a figure of merit. SNR is computed by
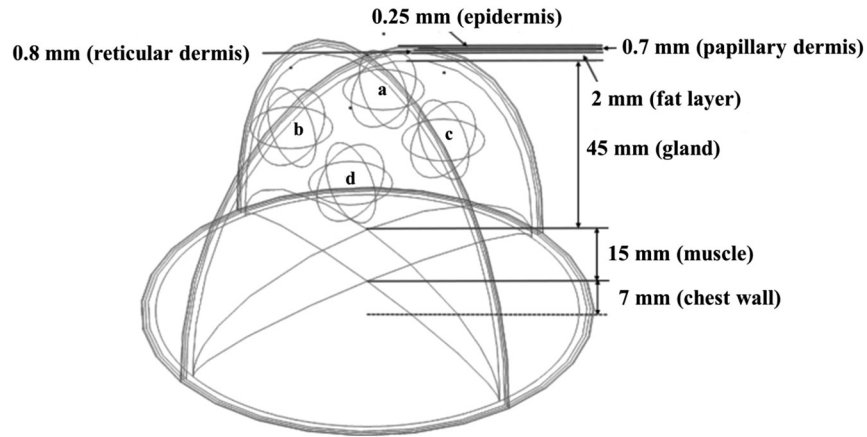
Fig. 4 The schematic of the modeled dense breast.

Table 2 Tumor depth from the surface.

Tumor	Depth (mm)
a	5.75
b	6.75
c	7.75
d	8.75

$$\text{SNR} = 20\,\text{Log}\left(\frac{\text{mean of tumor region} - \text{mean of sound region}}{\text{standard deviation of sound region}}\right)$$

$$\tag{10}$$

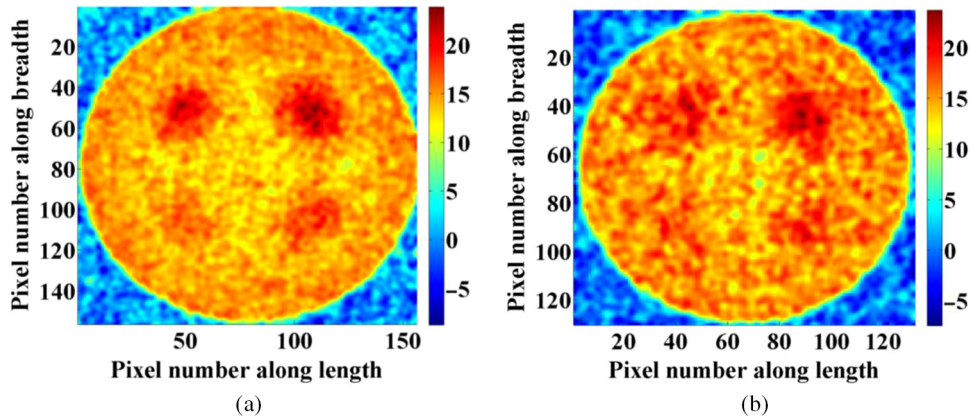Table 3 shows the calculated SNR values for all applied post-processing techniques obtained using LFMTWI and PT.

(a)   (b)

Fig. 5 Fitted noisy image: (a) with LFMTWI and (b) with PT.

(a)   (b)
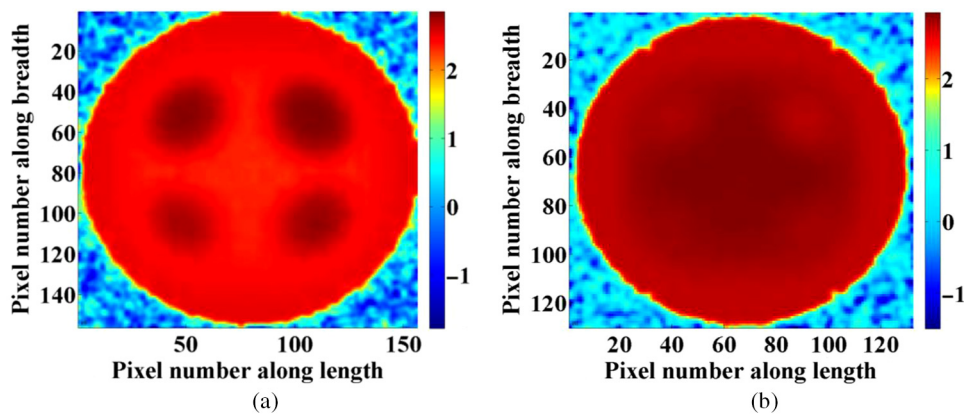
Fig. 6 Phase images obtained at a frequency of 0.004 Hz computed using Fourier transform: (a) with LFMTWI and (b) with PT.
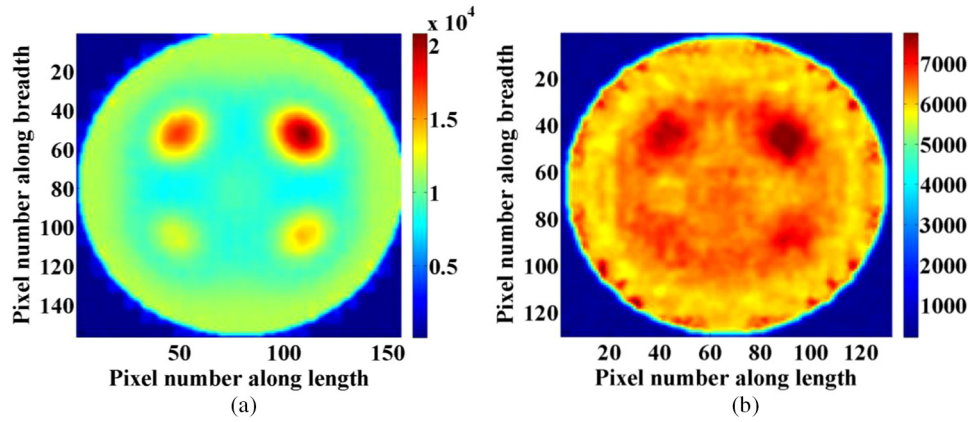
Fig. 7 Amplitude images obtained at a frequency of 0.004 Hz computed using Fourier transform: (a) with LFMTWI and (b) with PT.
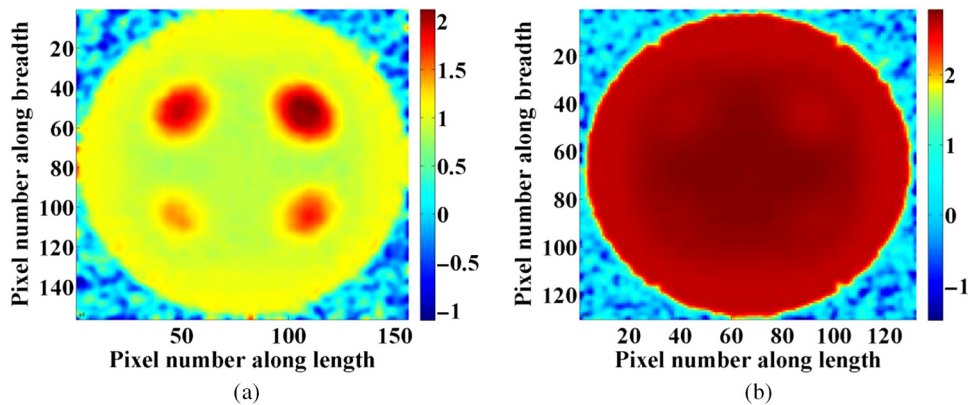

Fig. 8 Phase images computed using matched filter approach obtained at a time instant of: (a) 333 s with LFMTWI and (b) 543 s with PT.
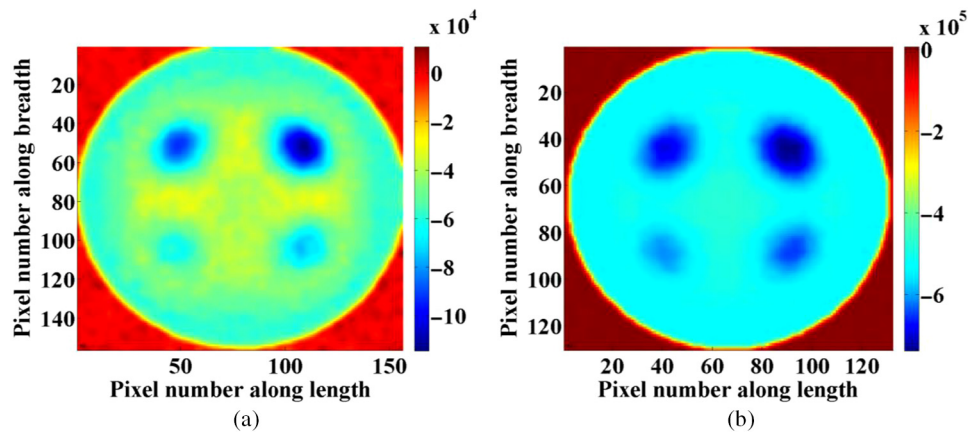

Fig. 9 Amplitude images computed using matched filter approach obtained at a time instant of: (a) 21 s with LFMTWI and (b) 822 s with PT.

CC peak amplitude versus depth of the tumor from the surface has been empirically fitted as shown in Fig. 10. This graph is shown for LFMTWI approach.

4.2 Modeling and Analysis of the Fatty Breast Tissue

The dimensional layout of the modeled fatty breast with each layer is shown in Fig. 11.

Here, the fat layer has a thickness of 67.5 mm, which makes it different from the dense breast and gland has thickness of 45 mm. Four tumors (denoted as a, b, c, and d in Fig. 11), each with 20 mm diameter, are placed at different depths as in dense breast. The respective depths in case of fatty breast are as given in Table 4.

Resultant images are constructed for both the approaches (LFMTWI and PT) and results are further compared by considering SNR as a figure of merit.

Table 3 Computed SNRs for dense breast.

| Resultant image →	Fitted noisy		FT phase		FT amplitude		Time-domain phase		Time-domain amplitude	
Heat flux →										
Tumor ↓	LFM	Pulse	LFM	Pulse	LFM	Pulse	LFM	Pulse	LFM	Pulse
A	24.3970	15.5576	83.5924	55.9579	90.1401	40.3323	95.2826	57.5852	97.5410	76.1571
B	22.6669	8.1771	82.4549	52.1136	83.1416	34.5850	91.7190	54.0593	90.5214	72.8336
C	21.3895	6.4873	79.9532	40.3897	73.6728	11.5876	85.3641	42.4366	83.2957	65.7893
D	17.6640	3.7826	77.7071	35.9439	64.4901	6.9087	77.1455	38.9958	75.4992	61.7965
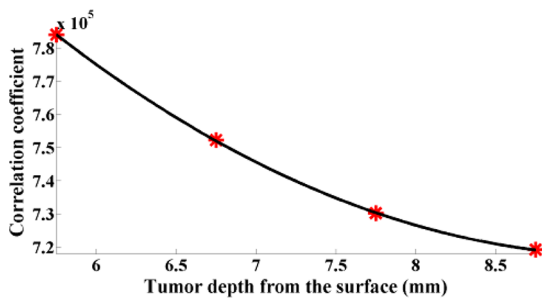
Fig. 10 CC peak amplitude of the tumor from the surface.

Table 4 Tumor depth from the surface.

Tumor	Depth (mm)
a	3.75
b	4.75
c	5.75
d	6.75

Image constructed from the fitted noisy data for fatty breast is as shown in Fig. 12(a) using LFMTWI and Fig. 12(b) using PT. The results obtained after processing the fitted noisy temporal profile while considering fatty breast are as shown in Figs. 13–16.

Figures 13(a) and 13(b) represent the phase images obtained at a frequency of 0.004 Hz reconstructed by applying Fourier transform on the fitted noisy temporal temperature profiles for LFMTWI and PT, respectively.

Figure 14. shows the amplitude images reconstructed by applying Fourier transform on the fitted noisy temporal temperature profiles. Figure 14(a) shows the reconstructed image using LFMTWI obtained at a frequency of 0.004 Hz and Fig. 14(b) using PT obtained at a frequency of 0.002 Hz.

The obtained matched filter-based phase and amplitude images are as shown in Figs. 15 and 16. Figure 15(a) shows the constructed phase image at the time instant of 141 s using LFMTWI and Fig. 15(b) is obtained at 448 s using PT approach whereas the amplitude image [Fig. 16(a)] is obtained at 131 s for LFMTWI and Fig. 16(b) obtained at 376 s for PT.

Results are further compared using SNR as a figure of merit. Table 5 shows the calculated SNR values for all applied post-processing techniques obtained using LFMTWI and PT.
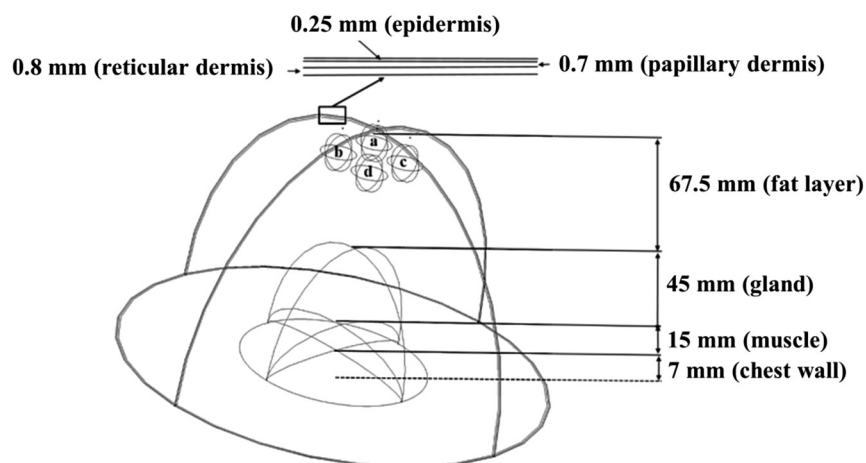
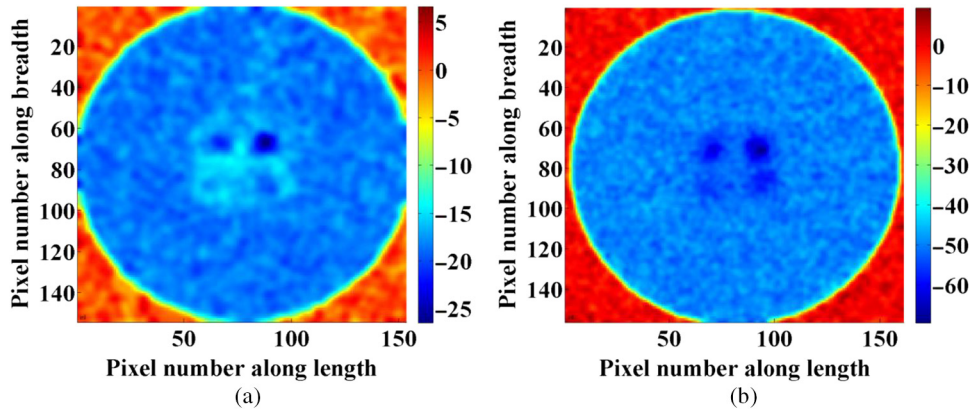**Fig. 11** The schematic of the modeled fatty breast.

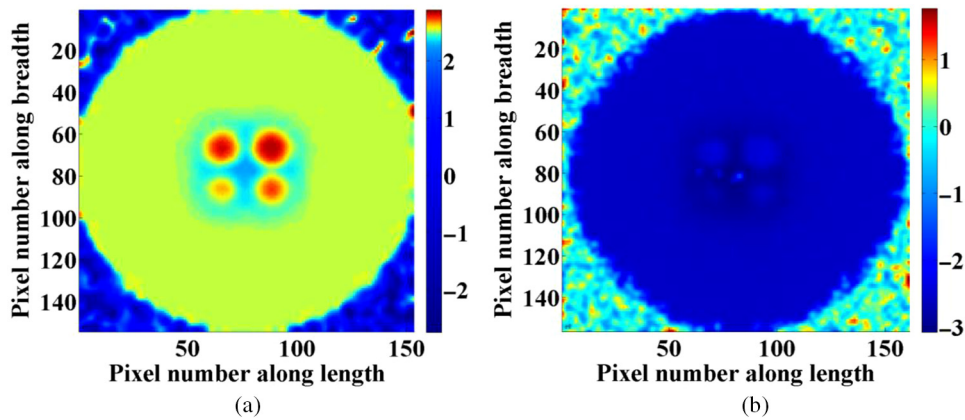**Fig. 12** Fitted noisy image: (a) with LFMTWI and (b) with PT.

Fig. 13 Phase images obtained at a frequency of 0.004 Hz computed using Fourier transform: (a) with LFMTWI and (b) with PT.
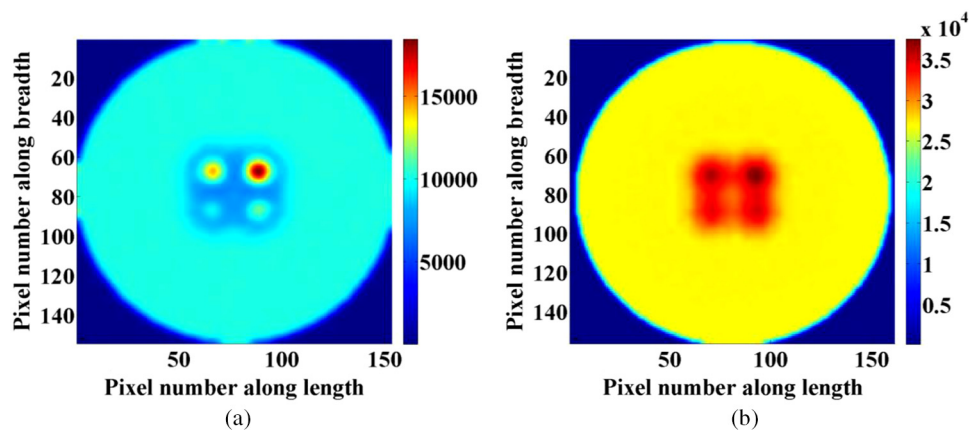

Fig. 14 Amplitude images computed using Fourier transform obtained at a frequency of: (a) 0.004 Hz with LFMTWI and (b) 0.002 Hz with PT.

CC peak amplitude versus depth of the tumor from the surface of the fatty breast has been empirically fitted as shown in Fig. 17. It shows that as the depth of the tumor from the surface increases CC decreases.

5 Conclusion

In this work, a 3-D model of the breast was introduced and simulated using an aperiodic thermal excitation scheme

(a)   (b)

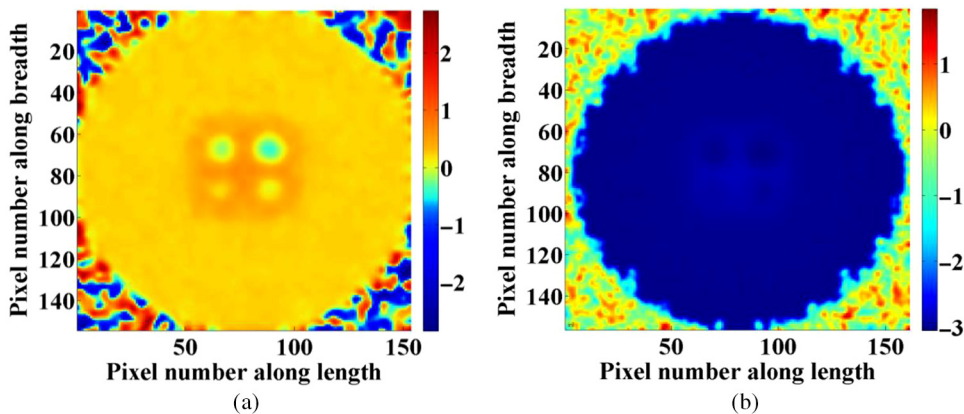**Fig. 15** Phase images computed using matched filter approach obtained at a time instant of: (a) 141 s with LFMTWI and (b) 448 s with PT.

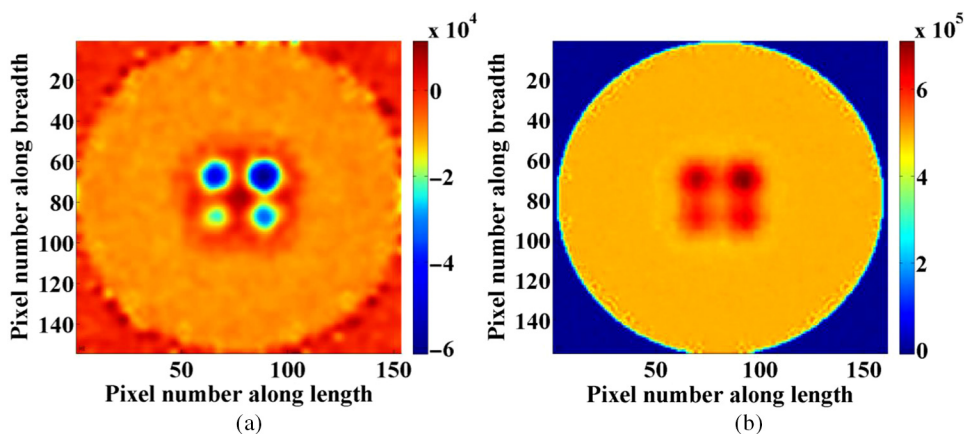(a)   (b)

Fig. 16 Amplitude images computed using matched filter approach obtained at a time instant of: (a) 131 s with LFMTWI and (b) 376 s with PT.

Table 5 Computed SNRs for fatty breast.

| Resultant image → | Fitted noisy | | FT phase | | FT amplitude | | Time-domain phase | | Time-domain amplitude | |
| Heat flux → | | | | | | | | | | |
Tumor ↓	LFM	Pulse	LFM	Pulse	LFM	Pulse	LFM	Pulse	LFM	Pulse
A	58.8886	22.6756	85.0903	56.7431	91.4664	74.7838	79.6221	64.7611	93.4652	77.6069
B	46.3714	15.7693	84.0656	54.9883	88.8571	70.8440	74.6534	61.5004	89.1135	74.0461
C	44.3998	10.9007	81.3584	53.3072	78.1171	65.5291	68.2060	56.5706	81.8909	67.8488
D	26.7616	2.4756	77.4901	47.5928	66.1416	61.7565	61.5136	48.1879	77.0979	60.5856
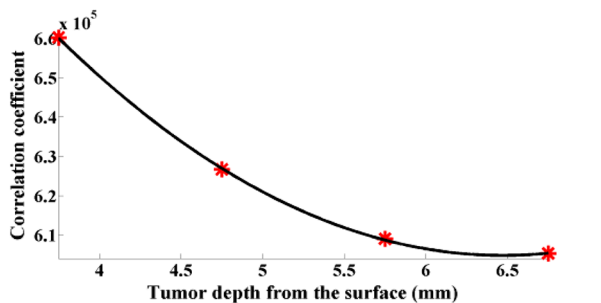
Fig. 17 CC peak amplitude versus depth of the tumor from the surface of the fatty breast.

for detection of breast cancer in fatty and dense breasts. The surface temperature distributions for tumors located at various depths are analyzed using frequency- and time-domain analysis schemes. Results obtained highlight the suitability of the proposed scheme and associated postprocessing methods for examining dense as well as fatty breasts for identification of tumors with improved detection resolution and sensitivity in comparison with the conventional pulse phase thermography. Furthermore, the obtained SNR supports the effectiveness of LFMTWI over the conventional widely used pulse phase thermography for breast cancer detection.

References

1. E. Y. K. Ng and E. C. Kee, "Advanced integrated technique in breast cancer thermography," *J. Med. Eng. Technol.* **32**, 2103–2114 (2007).
2. J. Koay, C. H. Herry, and M. Frize, "Analysis of breast thermography with artificial neural network," in *Proc. 26th IEEE EMBS Conf.*, San Francisco, California, pp. 1159–1162 (2004).
3. H. Usuki et al., "Relationship between thermographic observations of breast tumors and the DNA indices obtained by flow cytometry," *Biomed. Thermol.* **10**(4), 282–285 (1990).
4. X. P. V. Maldague, *Theory and Practice of Infrared Technology for Non Destructive Testing*, Wiley, New York (2001).
5. H. I. Ringermacher, D. R. Howard, and R. J. Filkins, "Flash-quenching for high resolution thermal depth imaging," in *AIP Conf. Proc.*, Vol. **700**, pp. 477–481 (2004).
6. G. Busse and P. Eyerer, "Thermal wave remote and nondestructive inspection of polymers," *Appl. Phys. Lett.* **43**(4), 355–357 (1983).
7. R. Mulaveesala and S. Tuli, "Implementation of frequency-modulated thermal wave imaging for non-destructive sub-surface defect detection," *Insight* **47**(4), 206–208 (2005).
8. R. Mulaveesala and S. Tuli, "Theory of frequency modulated thermal wave imaging for nondestructive subsurface defect detection," *Appl. Phys. Lett.* **89**(19), 191913 (2006).
9. V. S. Ghali, R. Mulaveesala, and M. Takei, "Frequency-modulated thermal wave imaging for non-destructive testing of carbon fiber-reinforced plastic materials," *Meas. Sci. Technol.* **22**(10), 104018 (2011).
10. R. Mulaveesala and G. Dua, "Non-invasive and non-ionizing depth resolved infra-red imaging for detection and evaluation of breast cancer: a numerical study," *Biomed. Phys. Eng. Express* **2**(5), 055004 (2016).
11. J. Liu et al., "Study of inspection on metal sheet with subsurface defects using linear frequency modulated ultrasound excitation thermal-wave imaging (LFM-UTWI)," *Infrared Phys. Technol.* **62**, 136–142 (2014).
12. J. Gong et al., "Investigation of carbon fiber reinforced polymer (CFRP) sheet with subsurface defects inspection using thermal-wave radar imaging (TWRI) based on the multi-transform technique," *NDTE Int.* **62**, 130–136 (2014).
13. E. Borazjani, D. Spinello, and D. S. Necsulescu, "Determination of the modulation frequency for thermographic non-destructive testing," *NDTE Int.* **70**(1), 1–8 (2015).
14. J. Liu et al., "Investigation on stress distribution of multilayered composite structure (MCS) using infrared thermographic technique," *Infrared Phys. Technol.* **61**, 134–143 (2013).
15. N. M. Sudarshan, E. Y. K. Ng, and S. I. Teh, "Surface temperature distribution of a breast with and without tumour," *Comput. Methods Biomech. Biomed. Eng.* **2**(3), 187–199 (1999).
16. H. H. Pennes, "Analysis of tissue and arterial blood temperatures in the resting human forearm," *J. Appl. Physiol.* **1**(2), 93–122 (1948).
17. E. Y. K. Ng and N. M. Sudharsan, "An improved three dimensional direct numerical modelling and thermal analysis, of a female breast with tumour," *Proc. Inst. Mech. Eng. H* **215**(1), 25–37 (2001).
18. A. Chanmugam, R. Hatwar, and C. Herman, "Thermal analysis of cancerous breast model," in *Proc. ASME Int. Mechanical Engineering Congress and Exposition (IMECE '12)*, Vol. 2, pp. 135–143 (2012).
19. M. M. Osman and E. M. Afify, "Thermal modeling of the normal woman's breast," *J. Biomech. Eng.* **106**, 123–130 (1984).
20. E. M. Afify, "Thermal modeling of the malignant woman's breast," *J. Biomech. Eng.* **110**(4), 269–276 (1988).
21. E. Y.-K. Ng, "A review of thermography as promising non-invasive detection modality for breast tumor," *Int. J. Therm. Sci.* **48**(5), 849–859 (2009).

Geetika Dua completed her schooling at Pratap Public School, Karnal. She received her BTech degree in electronics and communication engineering from Kurukshetra University, Kurukshetra, and her MTech degree in electronics and communication engineering from Guru Gobind Singh Indraprastha University, Delhi. Her major areas of research interest are the development of signal, image, and video processing methods for nondestructive testing/noninvasive imaging modalities for inspection of various industrial and biomedical materials.

Ravibabu Mulaveesala is an associate professor at the Indian Institute of Technology, Ropar. He received his MTech degree from the Regional Engineering College, Tiruchirappalli, and his PhD from the Indian Institute of Technology, Delhi, in 2000 and 2007, respectively. His research interests include thermal, acoustical, and optical methods for noninvasive/nondestructive imaging technologies. He serves as an editorial board member for several refereed journals from the Institute of Physics, Institute of Electrical and Electronics Engineers, and Elsevier.